Article

Photoreactions of Sc$_3$N@C$_{80}$ with Disilirane, Silirane, and Digermirane: A Photochemical Method to Separate I_h and D_{5h} Isomers

Masahiro Kako [1,*], Kyosuke Miyabe [1], Shinpei Fukazawa [1], Shinji Kanzawa [1], Masanori Yasui [1], Michio Yamada [2], Yutaka Maeda [2], Zdeněk Slanina [3,*], Filip Uhlík [4], Ludwik Adamowicz [5], Ilias Papadopoulos [6], Dirk M. Guldi [6,*], Makoto Furukawa [7], Shigeru Nagase [8] and Takeshi Akasaka [2,3,7,9]

[1] Department of Engineering Science, The University of Electro-Communications, Chofu 182-8585, Japan; miyabe@chemk.pc.uec.ac.jp (K.M.); fukazawa@chemk.pc.uec.ac.jp (S.F.); kanzawa@chemk.pc.uec.ac.jp (S.K.); myasui@uec.ac.jp (M.Y.)

[2] Department of Chemistry, Tokyo Gakugei University, Tokyo 184-8501, Japan; myamada@u-gakugei.ac.jp (M.Y.); ymaeda@u-gakugei.ac.jp (Y.M.); akasaka@tara.tsukuba.ac.jp (T.A.)

[3] School of Materials Science and Engineering, Huazhong University of Science and Technology, Wuhan 430074, China

[4] Department of Physical and Macromolecular Chemistry, Faculty of Science, Charles University, 128 43 Prague, Czech Republic; filip.uhlik@natur.cuni.cz

[5] Department of Chemistry and Biochemistry, University of Arizona, Tucson, AZ 85721-0041, USA; ludwik@email.arizona.edu

[6] Department of Chemistry and Pharmacy & Interdisciplinary Center for Molecular Materials, Friedrich-Alexander University Erlangen-Nürnberg, Egerlandstrasse 3, 91058 Erlangen, Germany; ilias.papadopoulos@fau.de

[7] Foundation for Advancement of International Science, Ibaraki 305-0821, Japan; furukawa@wellgreen.co.jp

[8] Fukui Institute for Fundamental Chemistry, Kyoto University, Kyoto 606-8103, Japan; nagase@ims.ac.jp

[9] TARA Center, University of Tsukuba, Tsukuba 305-8577, Japan

* Correspondence: m.kako@uec.ac.jp (M.K.); fromzdenek@yahoo.com (Z.S.); dirk.guldi@fau.de (D.M.G.)

Abstract: Under photoirradiation, Sc$_3$N@I_h-C$_{80}$ reacted readily with disilirane **1**, silirane **4**, and digermirane **7** to afford the corresponding 1:1 adducts, whereas Sc$_3$N@D_{5h}-C$_{80}$ was recovered without producing those adducts. Based on these results, we described a novel method for the exclusive separation of I_h and D_{5h} isomers of Sc$_3$N@C$_{80}$. The method includes three procedures: selective derivatization of Sc$_3$N@I_h-C$_{80}$ using **1**, **4**, and **7**, facile HPLC separation of pristine Sc$_3$N@D_{5h}-C$_{80}$ and Sc$_3$N@I_h-C$_{80}$ derivatives, and thermolysis of Sc$_3$N@I_h-C$_{80}$ derivatives to collect pristine Sc$_3$N@I_h-C$_{80}$. In addition, laser flash photolysis experiments were conducted to elucidate the reaction mechanism. Decay of the transient absorption of ^{3}Sc$_3$N@I_h-C$_{80}{}^*$ was observed to be enhanced in the presence of **1**, indicating the quenching process. When Sc$_3$N@D_{5h}-C$_{80}$ was used, the transient absorption was much less intensive. Therefore, the quenching of ^{3}Sc$_3$N@D_{5h}-C$_{80}{}^*$ by **1** could not be confirmed. Furthermore, we applied time-dependent density functional theory (TD-DFT) calculations of the photoexcited states of Sc$_3$N@C$_{80}$ to obtain insights into the reaction mechanism.

Keywords: metallofullerene; Sc$_3$N@C$_{80}$; disilirane; silirane; digermirane; density functional theory; photophysics

1. Introduction

Endohedral metallofullerenes (EMFs) have been investigated extensively because of their fascinating structures based on electron transfer from encapsulated metal species to carbon cages [1–17]. Among EMFs, trimetallic nitride template endohedral metallo-fullerenes (TNT-EMFs) constitute a major EMF family for which extensive studies have been conducted to ascertain and apply their remarkable properties [2,9,10]. In fact, Sc$_3$N@I_h-C$_{80}$ has been well studied among TNT-EMFs because of its high production yield [9]. A

few years after the discovery of Sc$_3$N@I_h-C$_{80}$, the D_{5h} isomer of Sc$_3$N@C$_{80}$ was isolated and characterized to demonstrate its higher reactivity than that of the I_h isomer [18,19]. For the synthesis of Sc$_3$N@C$_{80}$, however, separation of the I_h and D_{5h} isomers by high-performance liquid chromatography (HPLC) is not efficient because the retention times of these isomers are mutually similar using commercial HPLC columns.

To date, many chemical procedures without HPLC separation have been reported for separation of mixtures of fullerenes based on their chemical reactivity differences [20]. For example, Diels–Alder reactions using a cyclopentadiene-functionalized resin followed by retro-addition was used to facilitate the separation of the I_h and D_{5h} isomers of Sc$_3$N@C$_{80}$ and Lu$_3$N@C$_{80}$ [21]. Selective complexation procedures were developed using aminosilica and Lewis acids that precipitate with some EMFs [22,23]. These methods enabled separation of Sc$_3$N@I_h-C$_{80}$ in gram quantities. More recently, a selective oxidation procedure using a ferrocenium salt was applied to separate both isomers based on differences in their oxidation potentials. This procedure involves sequential column chromatographic separation of the unreactive Sc$_3$N@I_h-C$_{80}$ and the oxidized Sc$_3$N@D_{5h}-C$_{80}$, which were subsequently recovered by reduction [24]. Although Sc$_3$N@D_{5h}-C$_{80}$ and Sc$_3$N@C$_{68}$ were obtained as the same fraction in this method, it was subsequently reported that Sc$_3$N@D_{5h}-C$_{80}$ was separated from Sc$_3$N@C$_{68}$ based on the predominant reactivity of the latter in methano-derivatization using a tosyl hydrazone reagent [25].

For our ongoing study of fullerene chemistry, disilirane **1** has been used as a versatile derivatizing reagent [15,16]. In general, **1** reacts with EMFs efficiently under visible light to afford the corresponding silylated EMFs. Furthermore, EMFs that exhibit less negative first reduction potentials are reactive toward **1** under both thermal and photochemical conditions [15,16]. These results led us to examine the reactivity of Sc$_3$N@D_{5h}-C$_{80}$ for comparison with that of the corresponding I_h isomer. This report describes differences in the photochemical reactivities of the I_h and D_{5h} isomers of Sc$_3$N@C$_{80}$ toward **1** as well as silirane **4** [26,27] and digermirane **7** [28,29]. Very interestingly, Sc$_3$N@D_{5h}-C$_{80}$ was found to be photochemically inert toward **1**–**3**, whereas Sc$_3$N@I_h-C$_{80}$ undergoes facile addition reactions under identical conditions. This result indicates a novel photochemical method for the exclusive separation of the I_h and D_{5h} isomers of Sc$_3$N@C$_{80}$ as follows: (i) selective derivatization of Sc$_3$N@I_h-C$_{80}$ in mixtures of the I_h and D_{5h} isomers, (ii) facile HPLC separation of Sc$_3$N@D_{5h}-C$_{80}$ from the derivatized Sc$_3$N@I_h-C$_{80}$, and (iii) recovery of pristine Sc$_3$N@I_h-C$_{80}$ by thermolysis of its derivative.

In addition, the laser flash photolysis of Sc$_3$N@C$_{80}$ was conducted to elucidate differences in the reactivities of I_h and D_{5h} isomers. To date, few examples of comparative studies of the photoreactions of fullerene isomers with different cage symmetries have been reported. We reported earlier that C_{2v}-C$_{78}$ undergoes photoreaction with **1** to afford the corresponding silylated C$_{78}$, whereas D_3-C$_{78}$ was inert under the same conditions, indicating a procedure for the separation of C_{2v}-C$_{78}$ and D_3-C$_{78}$ [30]. More recently, the photodynamics of three isomers of Sc$_2$C$_2$@C$_{82}$ have been reported as depending on the different fullerene cage symmetries although the intermolecular reactions of the photoexcited Sc$_2$C$_2$@C$_{82}$ with organic molecules have not been examined yet [31]. For this study, we investigate the mechanistic origins for the difference in the reactivities of the Sc$_3$N@C$_{80}$ based on cage symmetries using spectroscopic and theoretical studies.

2. Results and Discussion

2.1. Separation of Sc$_3$N@I_h-C$_{80}$ and Sc$_3$N@D_{5h}-C$_{80}$ Using Photochemical Functionalization

As described above, earlier reports have shown that Sc$_3$N@I_h-C$_{80}$ reacts with **1** under photolytic conditions to give the corresponding 1,2-adduct **2** and 1,4-adduct **3** [32]. To examine the reactivity of Sc$_3$N@D_{5h}-C$_{80}$, a toluene solution of Sc$_3$N@D_{5h}-C$_{80}$ and **1** was irradiated for 20 h using two 500 W halogen lamps (cut off < 400 nm) under an argon atmosphere (Scheme 1). However, Sc$_3$N@D_{5h}-C$_{80}$ was found to be inert toward **1**, as shown in the HPLC profiles of the photoreaction (Figure S1 in Supplementary Materials).
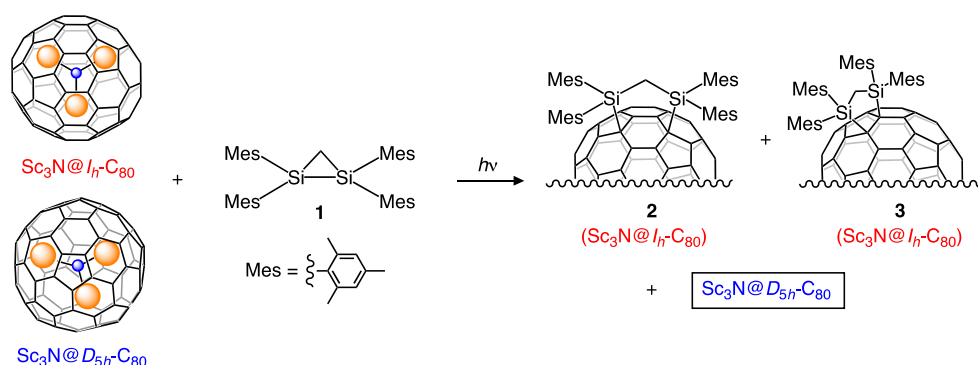
Scheme 1. Selective silylation of $Sc_3N@I_h$-C_{80} using **1**.

This result led us to apply this photoreaction to the separation of the I_h and D_{5h} isomers of $Sc_3N@C_{80}$. When a mixture of the I_h and D_{5h} isomers and **1** in toluene was irradiated for 40 h, the I_h isomer was consumed with the concomitant formation of **2** and **3**, whereas the D_{5h} isomer remained intact (Figure 1). The pristine $Sc_3N@D_{5h}$-C_{80} and the mixture of **2** and **3** were separated easily from the reaction mixture by preparative HPLC without recycling procedures. Finally, thermal desilylation of the mixture of **2** and **3** was performed at 160–170 °C in *o*-dichlorobenzene (ODCB) for 20 h. Subsequent HPLC separation afforded pristine $Sc_3N@I_h$-C_{80} (Figure S2). These procedures established a straightforward method to separate the I_h and D_{5h} isomers of $Sc_3N@C_{80}$.
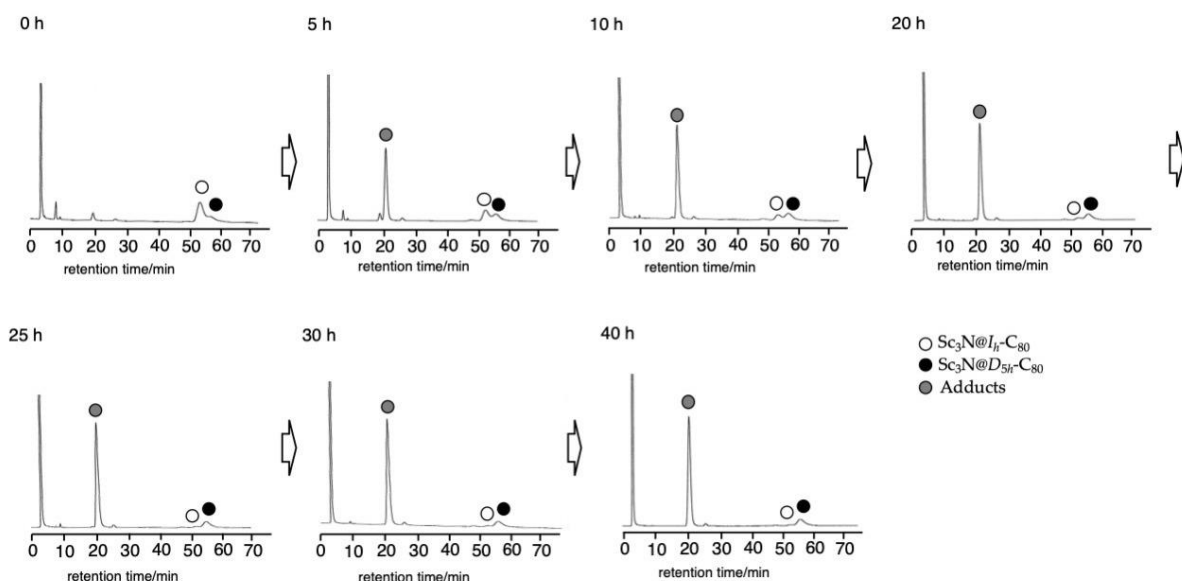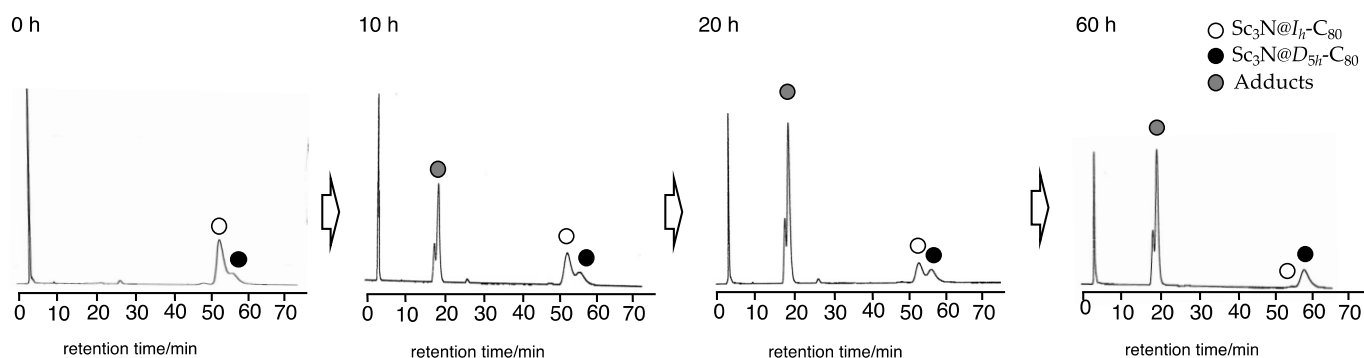

Figure 1. HPLC profiles of the reaction mixture in the photoreaction of $Sc_3N@I_h$-C_{80} and $Sc_3N@D_{5h}$-C_{80} with **1**. HPLC conditions: 5PBB column (ϕ 4.6 × 250 mm), eluent: toluene, flow rate: 1.0 mL/min, detection wavelength: 330 nm.

Such a separation method employing silirane **4** as an alternative derivatizing reagent was also examined based on our earlier reported result obtained from the photochemical addition of **4** to $Sc_3N@I_h$-C_{80} (Scheme 2) [26,27]. In fact, it was confirmed that **4** did not undergo an addition reaction with $Sc_3N@D_{5h}$-C_{80} under the photolytic condition used for $Sc_3N@I_h$-C_{80} (Figure S3). As expected, **4** also worked well as a selective carbosilylating reagent for $Sc_3N@I_h$-C_{80} without reaction with $Sc_3N@D_{5h}$-C_{80}. Consequently, photoirradiation of a mixture of the I_h and D_{5h} isomers and **4** in toluene for 60 h followed by HPLC separation gave pristine $Sc_3N@D_{5h}$-C_{80} and a mixture of **5a**, **5b**, and **6** [27], as shown in Figure 2. However, photochemical reactivity of **4** was somewhat lower than that of **1** considering the reaction time necessary to consume $Sc_3N@I_h$-C_{80}. In addition, thermal

decomposition of the mixture of **5a**, **5b**, and **6** was performed at 160–170 °C in ODCB for 40 h to give Sc$_3$N@I_h-C$_{80}$ along with a recovered mixture of **5a**, **5b**, and **6** (Figure S4). This result indicates that thermal extrusion reactions of the addends in **5a**, **5b**, and **6** were less efficient than those of **2** and **3**, which might reflect the relative stabilities of these adducts.
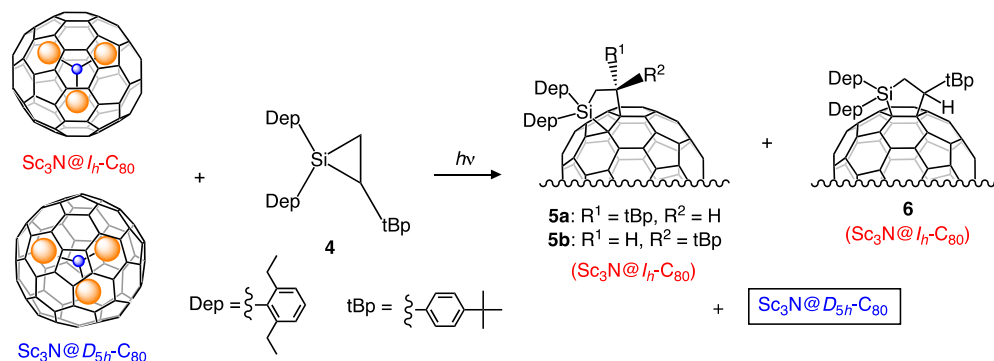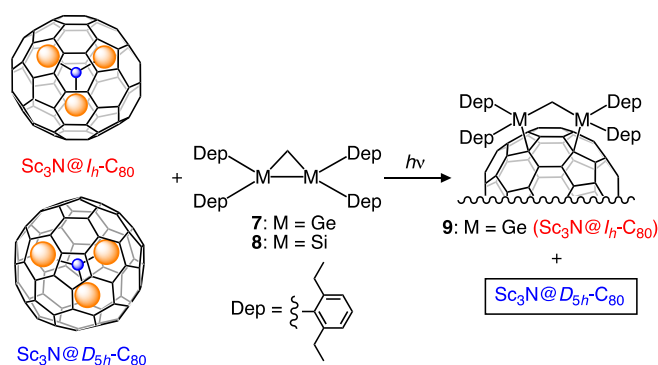

**Scheme 2.** Selective carbosilylation of Sc$_3$N@I_h-C$_{80}$ using **4**.

Figure 2. HPLC profiles of the reaction mixture in the photoreaction of Sc$_3$N@I_h-C$_{80}$ and Sc$_3$N@D_{5h}-C$_{80}$ with **4**. HPLC conditions: 5PBB column (ϕ 4.6 × 250 mm), eluent: toluene, flow rate: 1.0 mL/min, detection wavelength: 330 nm.

An earlier report described that digermirane **7** is more reactive than its silicon analog **8** toward Lu$_3$N@I_h-C$_{80}$ under visible irradiation because of the excellent electron-donor property of **7** [29]. This remarkable result led us to evaluate **7** as a third candidate for use as a selective derivatizing reagent for Sc$_3$N@I_h-C$_{80}$. First, the photoreaction of **7** with Sc$_3$N@I_h-C$_{80}$ was performed in a manner similar to that used for **1** and **4**. During photolysis, HPLC analysis indicated that a product peak developed intensively as the peak of Sc$_3$N@I_h-C$_{80}$ decreased (Figure S5). After consumption of Sc$_3$N@I_h-C$_{80}$, preparative HPLC separation of the reaction mixture afforded the 1,4-adduct **9** as the first example of germylated Sc$_3$N@I_h-C$_{80}$ derivative. The structure of **9** was established by X-ray crystallographic analysis as described below.

However, as expected, Sc$_3$N@D_{5h}-C$_{80}$ did not react with **7** under identical conditions for prolonged photoirradiation (Figure S6). This result led us to apply this germylation reaction to the separation of the I_h and D_{5h} isomers of Sc$_3$N@C$_{80}$ (Scheme 3). When a mixture of the I_h and D_{5h} isomers and **7** in toluene was irradiated for 20 h, the I_h isomer was consumed with the formation of **9**, whereas the D_{5h} isomer remained intact (Figure 3). The adduct **9** and the pristine D_{5h} isomer were separated easily using preparative HPLC. Finally, degermylation of **9** was accomplished by thermolysis at 130 °C in ODCB for 15 h (Figure S7). This thermolysis is apparently more efficient even at lower temperatures than in the cases of **2**, **3**, **5a**, **5b**, and **6**, probably because of the lower bond energies of C–Ge bonds (242 kcal/mol) than those of C–C and C–Si bonds (348 kcal/mol and 301 kcal/mol, respectively) [33].

**Scheme 3.** Selective germylation of Sc$_3$N@I_h-C$_{80}$ using **7**.
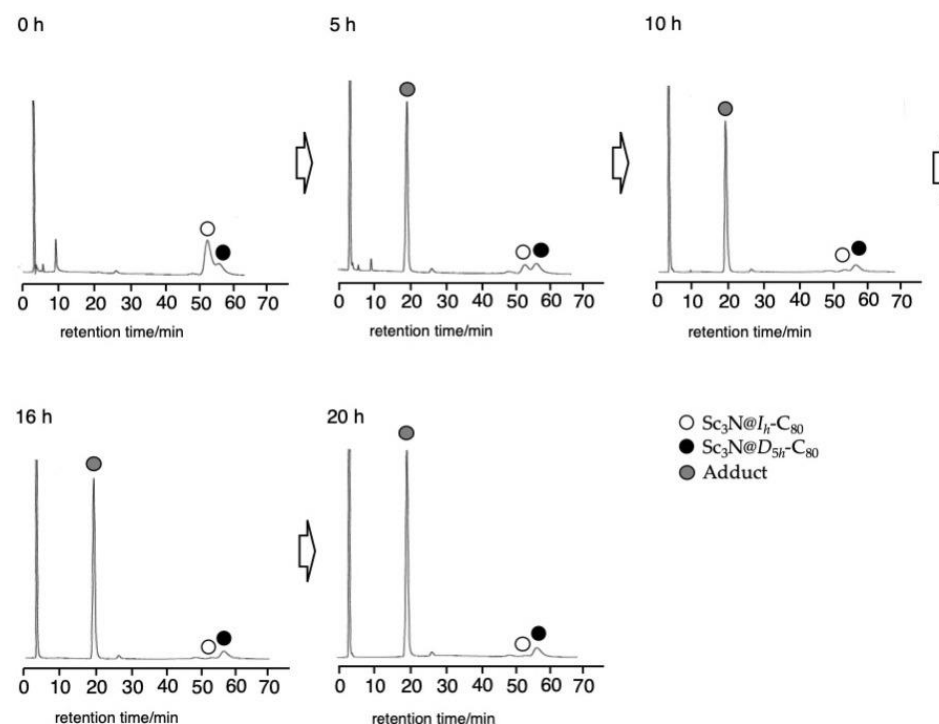
Figure 3. HPLC profiles of the reaction mixture in the photolysis of Sc$_3$N@I_h-C$_{80}$ and Sc$_3$N@D_{5h}-C$_{80}$ with **7**. HPLC conditions: 5PBB column (φ 4.6 × 250 mm), eluent: toluene, flow rate: 1.0 mL/min, detection wavelength: 330 nm.

2.2. Characterization of Germylated Sc$_3$N@I_h-C$_{80}$ **9**

Structural analysis of **9** was conducted based on our earlier studies of the related derivatives **2**, **10**, **11**, and **12** (Figure 4) [29,32]. The visible-near-IR (vis-NIR) spectrum of **9** closely resembles that of **2** (Figure 5). In addition, the NMR spectral features of **9** are similar to those of **11** and **12**. The existence of two isomeric molecules is inferred because the ^{1}H NMR spectrum shows two Ge-CH$_2$-Ge methylene groups, respectively, as singlets at 2.33 and 2.57 ppm (Figure S8). In the ^{13}C NMR spectrum, two methylene carbon signals that are attributable to Ge-CH$_2$-Ge were observed at 23.04 and 26.81 ppm. The ^{13}C NMR spectrum also shows two sets of four methyl groups, two sp^3 carbon signals of the I_h-C$_{80}$ cages, and a total of 102 sp^2 carbon signals that are attributable to the I_h-C$_{80}$ cages and the Dep ring carbons (Figure S9). These results indicate the existence of a mixture of conformational isomers of 1,4-adducts with C_2 symmetries, as observed for **2**, **10**, **11**, and **12**. To examine the conformational exchange in **9**, variable temperature (VT) ^{1}H NMR experiments were performed between 303 and 363 K (Figure S10). As expected, the signals coalesced as the temperatures increased to show broad signals at 363 K. The spectrum at 303 K was reproduced when the NMR probe temperature was

decreased to room temperature. The matrix-assisted laser desorption ionization time-of-flight (MALDI-TOF) mass spectrum showed that no molecular ion peak expected for 9^- was observed, although 1,1,4,4-tetraphenyl-1,3-butadiene (TPB), 9-nitroanthracene (9-NA), and 2,5-dihydroxybenzoic acid (DHB) were used as matrices. This result is attributable to the low stability of the molecular ion 9^-, as reported for the MALDI-TOF spectrum of **12** [29].
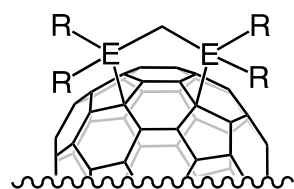
10: E = Si, R = Mes
11: E = Si, R = Dep
**12**: E = Ge, R = Dep

Figure 4. $Lu_3N@I_h$-C_{80}-based 1,4-adducts.
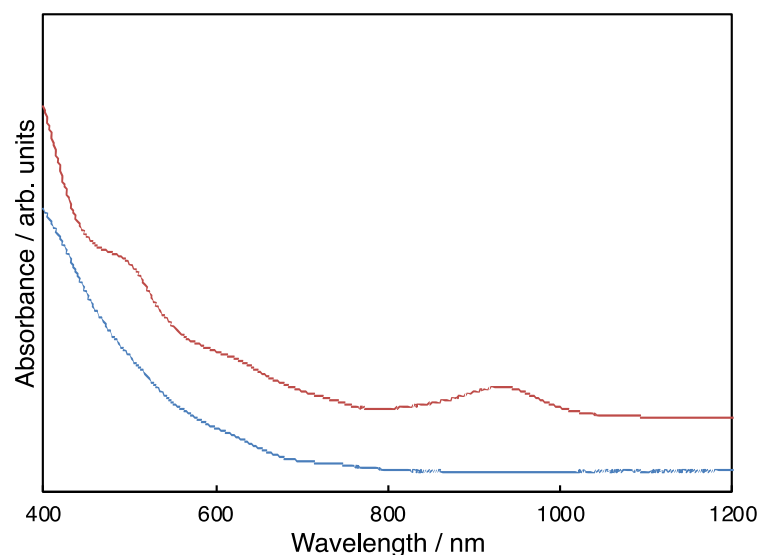
Figure 5. Vis–NIR absorption spectra of **9** (red) and $Sc_3N@I_h$-C_{80} (blue) in CS_2.

Fortunately, the 1,4-addition structure of **9** was determined firmly using the following X-ray crystallographic analysis. Black block crystals of **9** suitable for X-ray diffraction were obtained using the liquid–liquid bilayer diffusion method with CS_2 and hexane at 0 °C. The crystal structure of **9** shows two disordered positions in the I_h-C_{80} cage with occupancies of 0.72 and 0.28, whereas the digermirane addend is ordered (Figure S11). This result suggests that the crystal structure of **9** includes a pair of diasteromers, which is consistent with the NMR observations. Disorder also exists in the orientations of the Sc_3N clusters. They involve six locations of Sc atoms with a common N atom position. These Sc atom sites fall into two Sc_3N sets with occupancies of 0.68 and 0.32. Figure 6 presents orientation of the cage and the Sc_3N cluster in **9** with major occupancies.

We have already reported that the redox properties of silylated and germylated EMFs are altered considerably compared to the corresponding pristine fullerenes because of electron-donating effects of the silyl and germyl groups [16]. The redox property of **9** was verified using cyclic voltammetry (CV) and differential pulse voltammetry (DPV), as shown in Figure 7. The first oxidation (E^{ox}_1) and first reduction (E^{red}_1) potentials of **9** are shifted cathodically by 510 and 250 mV, respectively, relative to those of $Sc_3N@I_h$-C_{80} as presented in Table 1. In addition, both E^{ox}_1 and E^{red}_1 potentials of **9** are slightly more negative than those of the silylated derivative **2** [32]. Furthermore, the density functional

theory calculations of **9** were conducted at the B3LYP/6-31G*~SDD level to obtain a basis for its electronic structure [34–37]. The optimized structure of **9** was calculated using an initial structure resembling that of the X-ray structure, as shown in Figure 6. The highest occupied molecular orbital (HOMO) and the lowest unoccupied molecular orbital (LUMO) levels of **9** are higher than those of pristine $Sc_3N@I_h$-C_{80} by 0.68 and 0.45 eV, respectively (Table 1). These changes of the HOMO and LUMO levels are qualitatively consistent with those of the redox potentials of **2** and $Sc_3N@I_h$-C_{80}.
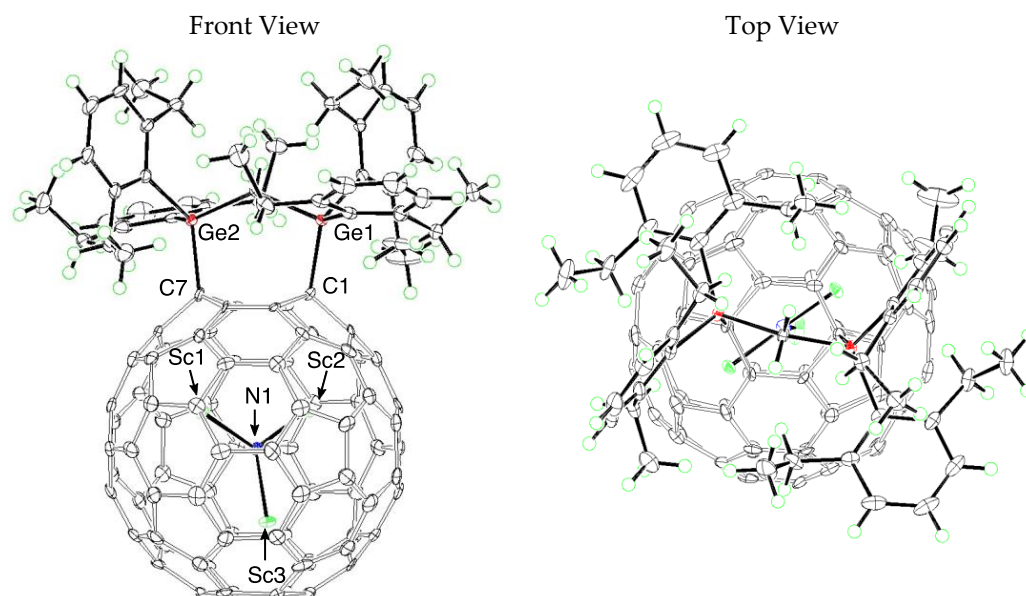
Figure 6. ORTEP drawings of **9** showing thermal ellipsoids at the 50% probability level at 120 K. The CS_2 molecule is omitted for clarity.
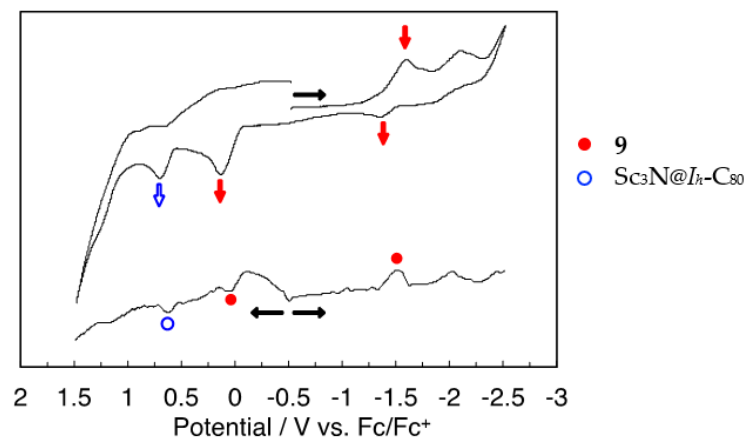
Figure 7. Cyclic voltammograms (CV) and differential pulse voltammograms (DPV) of **9** in ODCB containing 0.1 M (*n*-Bu)$_4$NPF$_6$. Conditions: working electrode, a glassy carbon electrode; counter-electrode, Pt wire; reference electrode, SCE; CV scan rates, 20 mV/s; DPV scan rate, 50 mV/s.

Table 1. Redox potentials (V) ^{a} and calculated HOMO/LUMO levels (eV) of **2**, **9**, and $Sc_3N@I_h$-C_{80}.

Compound	E^{ox}_1	E^{red}_1	HOMO	LUMO
9	+0.06 ^{b}	−1.51	−4.82	−2.85
2	+0.08 ^{b,c}	−1.45 ^{c}	−4.81	−2.84
$Sc_3N@I_h$-C_{80}	+0.57 ^{d}	−1.26 ^{d}	−5.50	−3.30

^{a} Values obtained by DPV are in volts relative to the ferrocene/ferrocenium couple (Fc/Fc$^+$). ^{b} Irreversible. ^{c} Data from Ref. [32]. ^{d} Data from Ref. [21].

2.3. Transient Absorption Spectroscopy of Photoreactions of Sc$_3$N@C$_{80}$

Laser flash photolysis experiments were conducted to shed light on the differences in the reactivities of the I_h and D_{5h} isomers. Transient absorption spectra were observed in visible (420–760 nm) and NIR (810–1028 nm, 1055–1400 nm) regions using laser excitation at 387 nm. The gaps in the probed spectral range stem from the detection limits of the visible and NIR detectors, gap between 760 and 810 nm, and from the fundamental wavelength of the white light laser source, gap between 1028 and 1055 nm. In toluene, the absorption band of the triplet excited state of Sc$_3$N@I_h-C$_{80}$ (^{3}Sc$_3$N@I_h-C$_{80}$*) was observed at λ_{max} 520 nm, as shown in Figures 8 and S12. A report of an earlier study described how the singlet excited state of Sc$_3$N@I_h-C$_{80}$ (^{1}Sc$_3$N@I_h-C$_{80}$*) undergoes facile intersystem crossing (ISC) to give ^{3}Sc$_3$N@I_h-C$_{80}$* with an absorption band around 500 nm [38]. Upon addition of 200 times equimolar amounts of **7**, the decay of ^{3}Sc$_3$N@I_h-C$_{80}$* was accelerated considerably, as shown in comparisons of decay plots both at 500 nm (Figure 9a,b) and at 1104 nm (Figure 9c,d).
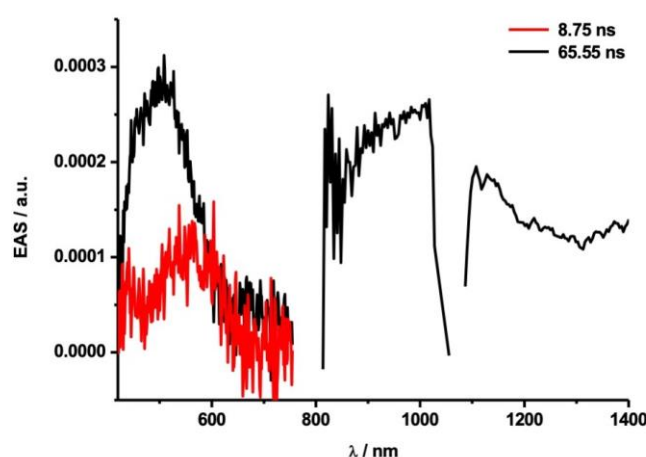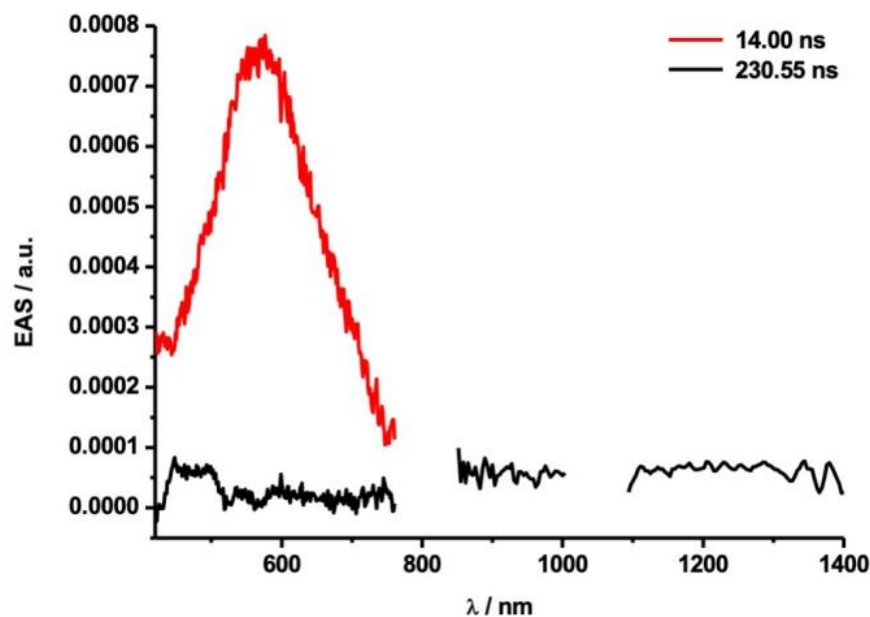

Figure 8. Evolution-associated spectra (EAS) obtained by the photolysis of Sc$_3$N@I_h-C$_{80}$ (λ_{ex} = 387 nm, E = 400 nJ; Figure S12) at their respective relative delay times. The transient absorption of the triplet excited state of Sc$_3$N@I$_h$-C$_{80}$ is shown in black and for toluene in red.

However, when Sc$_3$N@D_{5h}-C$_{80}$ was photolyzed under the same conditions, the observed transient absorption peak was much weaker than in the case of Sc$_3$N@I_h-C$_{80}$, as shown in Figures 10 and S14. Singlet and triplet excited states of Sc$_3$N@D_{5h}-C$_{80}$ (^{1}Sc$_3$N@D_{5h}-C$_{80}$* and ^{3}Sc$_3$N@D_{5h}-C$_{80}$*, respectively) have not been hitherto characterized by spectroscopic studies. Therefore, several mechanistic possibilities should be examined for the weak transient absorption in Figure 10. For example, the photoexcitation of Sc$_3$N@D_{5h}-C$_{80}$ might not be as efficient as that of Sc$_3$N@I_h-C$_{80}$, although the former has a lower but comparable molar extinction coefficient at λ = 387 nm (excitation wavelength in laser flash photolysis) compared to that of the latter, as shown in Figure S16. Alternatively, if it is assumed that the molar extinction coefficient and the lifetime of ^{3}Sc$_3$N@D_{5h}-C$_{80}$* is not significantly different from those of ^{3}Sc$_3$N@I_h-C$_{80}$*, then the weak absorption observed in Figure 10 suggests the low concentration of ^{3}Sc$_3$N@D_{5h}-C$_{80}$* under photolytic conditions. One possible explanation for this point is that the ISC process from ^{1}Sc$_3$N@D_{5h}-C$_{80}$* to ^{3}Sc$_3$N@D_{5h}-C$_{80}$* might be less effective than in the case of Sc$_3$N@I_h-C$_{80}$. In the presence of 200 times equimolar amounts of **7**, no appreciable difference in intensity of the transient absorption at 500 nm was observed because intense absorption of the triplet excited state of toluene hindered the evaluation (Figure 11a,b) [39]. Although slight differences of intensity at 1215 nm were noted upon addition of **7** (Figure 11c,d), they are mostly attributable to the poor signal-to-noise ratio caused by the low intensity in the NIR region. As such, a quantitative analysis of the photoactivity of Sc$_3$N@D_{5h}-C$_{80}$ and, in turn, a comparison with Sc$_3$N@I_h-C$_{80}$ is rendered impossible.
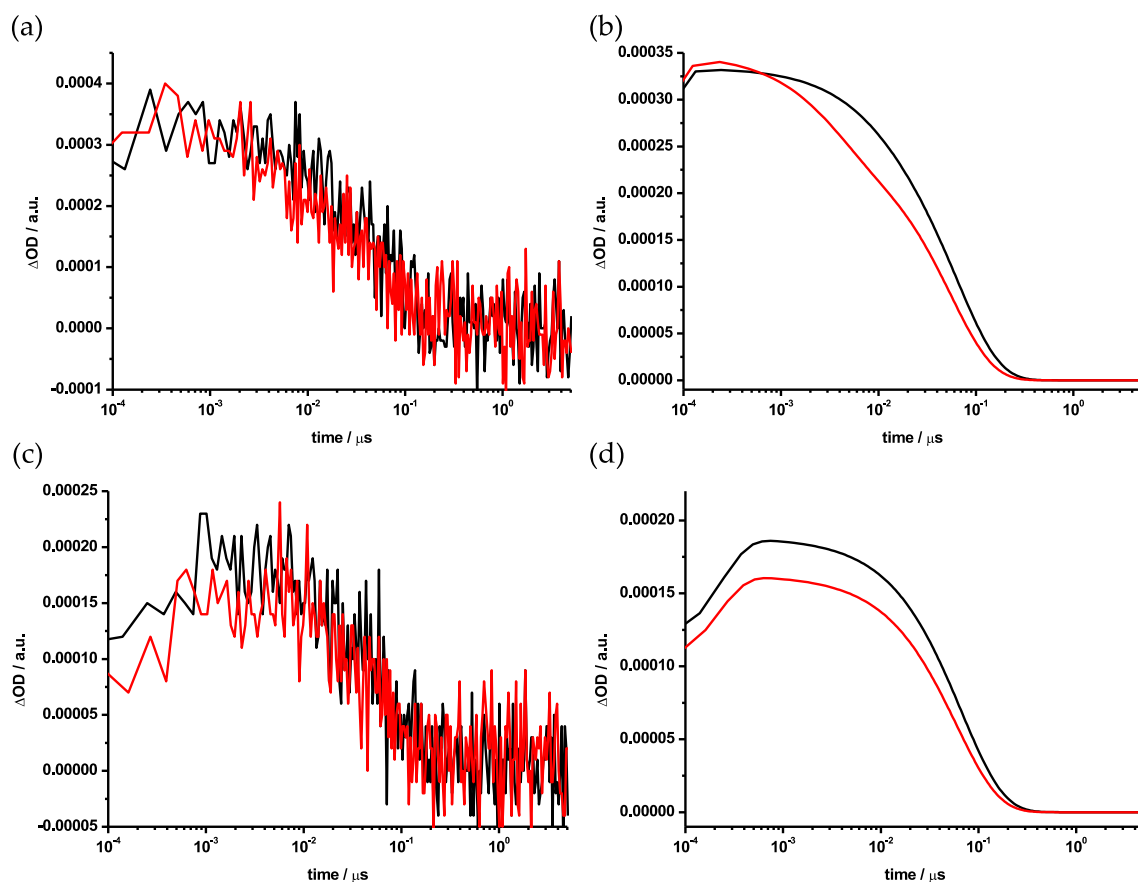
Figure 9. Decay profiles of transient absorption (Figures 8 and S12) using Sc$_3$N@I_h-C$_{80}$ in the absence (black) and the presence (red) of 200 times equimolar amounts of **7**: (**a**) observed traces at 500 nm and (**b**) fitting plots, (**c**) observed traces at 1104 nm and (**d**) fitting plots. The residuals of the decay profiles are located in the supporting information (Figure S13).

Figure 10. Evolution-associated spectra (EAS) obtained by the photolysis of Sc$_3$N@D_{5h}-C$_{80}$ (λ_{ex} = 387 nm, E = 400 nJ; Figure S14) at their respective relative delay times. The transient absorption of the triplet excited state of Sc$_3$N@D_{5h}-C$_{80}$ is shown in black and for toluene in red.
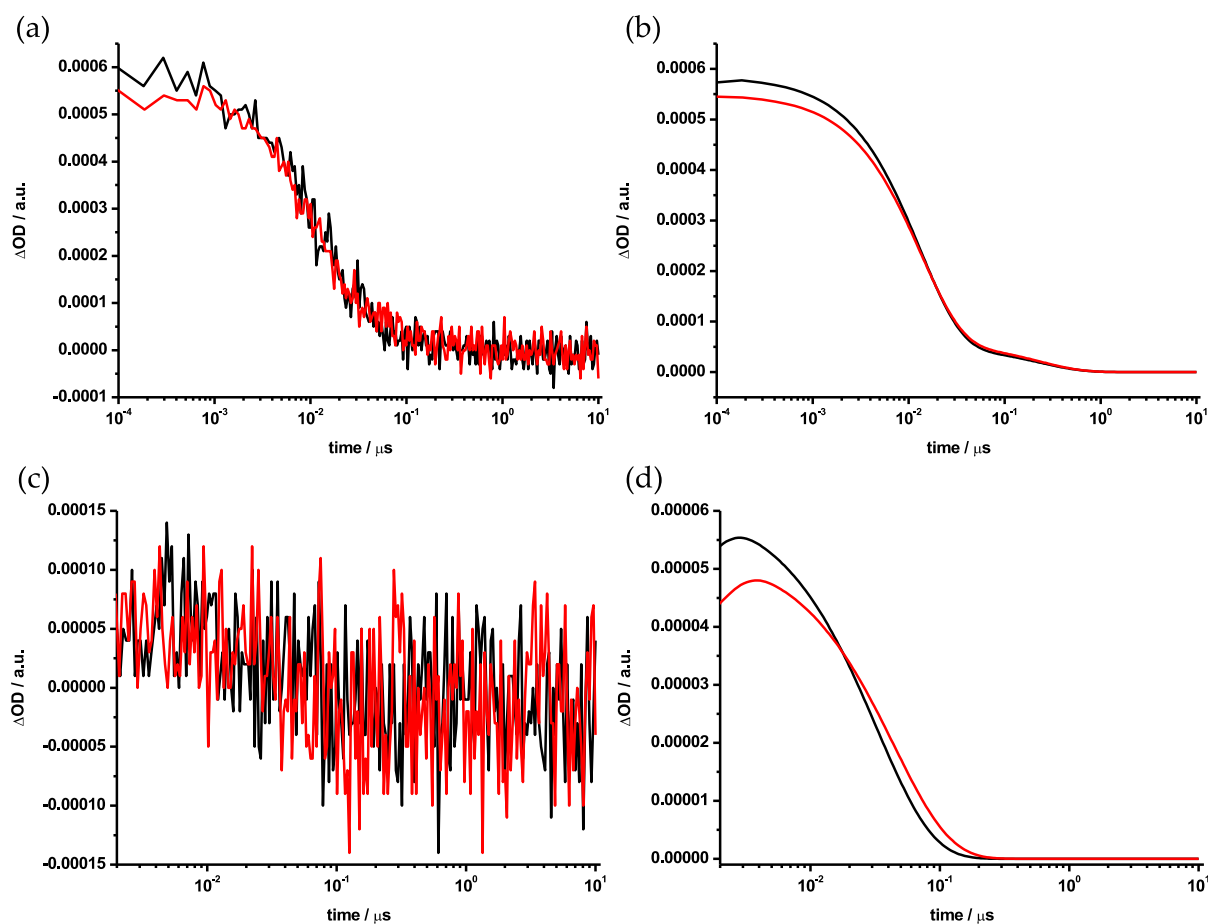
Figure 11. Decay profiles of transient absorption (Figures 10 and S14) using Sc$_3$N@D_{5h}-C$_{80}$ in the absence (black) and the presence (red) of 200 times equimolar amounts of **7**: (**a**) observed traces at 500 nm and (**b**) fitting plots, (**c**) observed traces at 1215 nm and (**d**) fitting plots. The residuals of the decay profiles are located in the supporting information (Figure S15).

2.4. Theoretical Calculations of Photoreactions of Sc$_3$N@C$_{80}$

To gain insight into the photochemical processes of Sc$_3$N@C$_{80}$, we applied time-dependent density functional theory (TD-DFT) [40] calculations on the ten lowest excited states including the singlet states (S$_n$; n = 1, 2, . . .) and triplet states (T$_n$; n = 1, 2, . . .), respectively, for the I_h and D_{5h} isomers of Sc$_3$N@C$_{80}$. The corresponding electronic excitation energies are schematized in Figure 12. Major orbital transition configurations are presented in Tables S1 and S2.

According to Kasha's rule [41], when the energy gaps between two singlet states (S$_n$ and S$_m$) are small, internal conversion (IC) processes from energetically higher singlet states to lower singlet states are enhanced more effectively than the ISC processes. In the case of Sc$_3$N@I_h-C$_{80}$, there are the triplet excited states T$_2$ and T$_3$, with energies closely approximating those of the lowest singlet excited state S$_1$. The energy differences between S$_1$-T$_2$ and S$_1$-T$_3$ are, respectively, 0.0387 and 0.0381 eV (Figure 12a). In the case of Sc$_3$N@D_{5h}-C$_{80}$, T$_1$ is energetically lower than S$_1$, which is lower than other triplet states T$_n$ (n > 1). S$_1$ and T$_1$ are different from each other in energy by 0.1239 eV (Figure 12b). However, these energy differences do not explain the efficiencies of the ISC processes in Sc$_3$N@C$_{80}$. Alternatively, the efficiency of the ISC processes might depend on the spin-orbit coupling (SOC) interaction between the singlet and triplet excited states. The behaviors of encapsulated metal clusters inside the carbon cages might therefore affect enhancement of the SOC interaction. Further understanding of the photoreactivities of Sc$_3$N@C$_{80}$ must await investigations of those photoexcited states of the corresponding I_h and D_{5h} isomers.
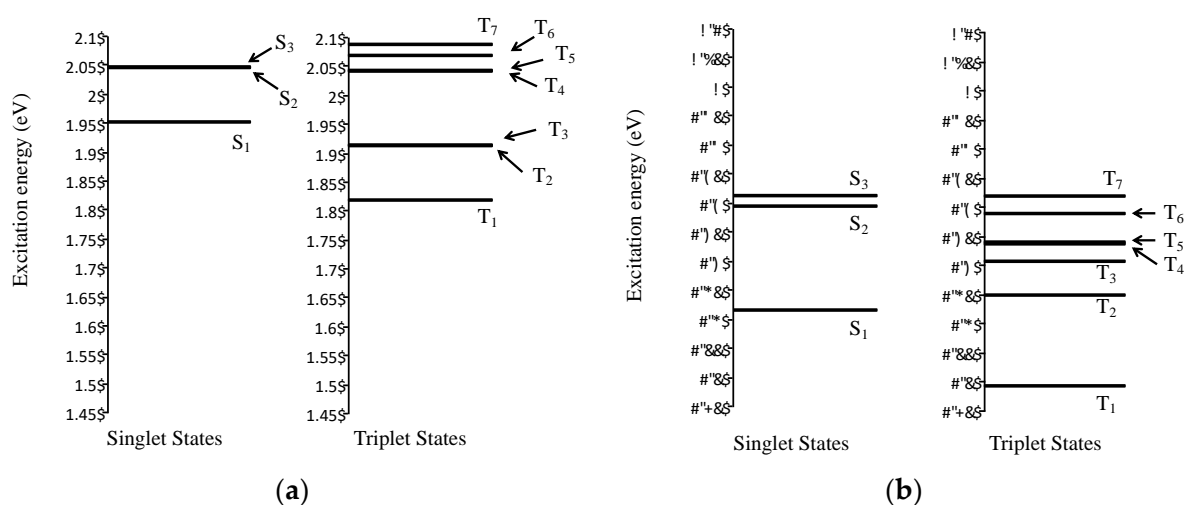
Figure 12. Calculated energies of singlet and triplet excited states of (**a**) Sc$_3$N@I_h-C$_{80}$ and (**b**) Sc$_3$N-@D_{5h}-C$_{80}$.

It was proposed in an earlier report of the relevant literature that the photoreaction of C$_{60}$ and **1** proceeds via the electron donor–acceptor interaction between ^{3}C$_{60}$* and **1** based on a quenching experiment of ^{3}C$_{60}$* by **1** [42]. The Rehm–Weller equation [43,44] for estimating the free energy change ΔG of electron transfer (ET) between **1** and ^{3}C$_{60}$* in non-polar solvents such as toluene exhibited a positive value. Therefore, results suggest that the ET between **1** and ^{3}C$_{60}$* is not efficient in non-polar solvents, but that process is regarded as possible because the ΔG value is not so large [42]. Additionally, it has been reported that photoirradiation of C$_{60}$ and siliranes that possess benzylsilane structures, which are good electron donors, afforded the corresponding adducts [45]. In contrast, when siliranes without benzylsilane structures were used as substrates, the photoaddition reaction proceeded very slowly.

Based on these results, the ΔG values for the ET processes from **1** to the excited triplet states of Sc$_3$N@I_h-C$_{80}$ and Sc$_3$N@D_{5h}-C$_{80}$ were calculated using the oxidation potential (E_{ox}) of **1** (+0.27 V vs. Fc/Fc$^+$) [42] and the first reduction potentials (E_{red}^1) of Sc$_3$N@I_h-C$_{80}$ (−1.26 V vs. Fc/Fc$^+$) [21] and Sc$_3$N@D_{5h}-C$_{80}$ (−1.33 V vs. Fc/Fc$^+$) [21], respectively. Assuming that the IC process from higher excited triplet states T$_n$ (n >1) to the lowest state T$_1$ occurs rapidly, the energies of the T$_1$ states were evaluated using TD-DFT calculations as 1.82 eV for Sc$_3$N@I_h-C$_{80}$ and 1.49 eV for Sc$_3$N@D_{5h}-C$_{80}$. As a result, the ΔG values were estimated as +10.36 kcal/mol for Sc$_3$N@I_h-C$_{80}$ and +19.50 kcal/mol for Sc$_3$N@D_{5h}-C$_{80}$ [43,46,47]. These values are positive, as in the case of C$_{60}$, but the value of the I_h isomer is small, whereas that of the D_{5h} isomer is nearly twice as large as that of the I_h isomer. These results suggest that the photoinduced electron transfer process of ^{3}Sc$_3$N@D_{5h}-C$_{80}$* should be less efficient than that of ^{3}Sc$_3$N@I_h-C$_{80}$* even if they take place. Based on these estimations, the poor electron acceptor property of ^{3}Sc$_3$N@D_{5h}-C$_{80}$* might decrease its photochemical reactivity toward **1**, **4**, and **7**.

3. Experimental Section

Separation of Sc$_3$N@C$_{80}$ using **1**: A mixture of the I_h and D_{5h} isomers of Sc$_3$N@C$_{80}$ (2.7 mg) and **1** (58 mg) in toluene (20 mL) was degassed using freeze–pump–thaw cycles under reduced pressure in a Pyrex tube (ϕ20 mm). The solution was irradiated for 40 h with two 500 W halogen lamps using an aqueous sodium nitrite filter solution (cutoff < 400 nm) under an argon atmosphere. Preparative HPLC separation with a Buckyprep-M column of the reaction mixture afforded pristine Sc$_3$N@D_{5h}-C$_{80}$ (0.7 mg) and a mixture of **2** and **3** (2.2 mg).

Thermal desilylation of **2** and **3**: A solution of **2** and **3** (2.1 mg) in ODCB (5 mL) was heated at 160–170 °C under an argon atmosphere in a Schlenk tube in the dark for 20 h.

After removal of ODCB in vacuo, Sc$_3$N@I_h-C$_{80}$ (0.8 mg) was obtained by preparative HPLC separation with a Buckyprep-M column.

Selective carbosilylation of Sc$_3$N@C$_{80}$ using **4**: A mixture of I_h and D_{5h} isomers of Sc$_3$N@C$_{80}$ (2.6 mg) and **4** (61 mg) in toluene (20 mL) was irradiated as described above for 60 h. Preparative HPLC separation with a Buckyprep-M column of the reaction mixture afforded pristine Sc$_3$N@D_{5h}-C$_{80}$ (0.5 mg) and a mixture of **5a**, **5b**, and **6** (2.5 mg).

Thermal decarbosilylation of **5a**, **5b**, and **6**: A solution of **5a**, **5b**, and **6** (2.1 mg) in ODCB (5 mL) was heated at 160–170 °C under an argon atmosphere in a Schlenk tube in the dark for 40 h. After removal of ODCB in vacuo, Sc$_3$N@I_h-C$_{80}$ (0.9 mg) was obtained along with a recovered mixture of **5a**, **5b**, and **6** (0.7 mg) by preparative HPLC separation with a Buckyprep-M column.

Photoreaction of Sc$_3$N@I_h-C$_{80}$ with **7**: A solution of Sc$_3$N@I_h-C$_{80}$ (2.0 mg) and **7** (12.6 mg) in toluene (15 mL) was irradiated for 5 h as described above. Preparative HPLC separation with a Buckyprep-M column of the reaction mixture afforded **9** (2.1 mg). Spectral data for **9**: The following NMR data are described based on the existence of two conformational isomers with C_2 symmetries. ^{1}H NMR (500 MHz, CS$_2$/CDCl$_3$ (1:1), 298 K) δ 7.33–7.28 (m, 6H), 7.22 (t, J = 7.5 Hz, 2H), 7.18 (d, J = 7.5 Hz, 2H), 7.13 (d, J = 7.5 Hz, 2H), 7.10 (t, J = 7.5 Hz, 2H), 7.02–6.96 (m, 8H), 6.91 (d, J = 7.5 Hz, 2H), 3.75 (dq, J = 7.5 Hz, 15 Hz, 2H), 3.68–3.43 (m, 8H), 3.31 (dq, J = 7.5 Hz, 15 Hz, 2H), 3.09 (dq, J = 7.5 Hz, 15 Hz, 2H), 2.98–2.74 (m, 8H), 2.63 (dq, J = 7.5 Hz, 15 Hz, 2H), 2.57 (s, 2H), 2.51–2.36 (m, 8H), 2.33 (s, 2H), 1.70 (t, J = 7.5 Hz, 6H), 1.43 (t, J = 7.5 Hz, 6H), 0.82 (t, J = 7.5 Hz, 6H), 0.76 (t, J = 7.5 Hz, 6H), 0.66–0.63 (m, 18H), 0.58 (t, J = 7.5 Hz, 6H); ^{13}C NMR (125 MHz, CS$_2$/CDCl$_3$ (1:1), 298 K) δ 178.97, 176.15, 153.01, 152.92, 152.67, 152.58, 151.85, 151.68, 150.91, 150.87, 149.81, 149.67, 149.06, 148.45(2set), 147.72, 147.62, 147.42, 147.27, 147.22, 147.05, 147.00, 146.85, 146.67, 146.56, 146.52, 146.45, 146.38, 145.91, 146.88, 145.55, 145.52, 145.44, 145.36, 145.23, 144.97, 144.78, 144.58, 144.32, 143.16, 142.75, 142.37, 142.24, 141.95, 141.75, 141.15, 141.06, 140.88, 140.74, 140.64, 140.54, 140.45, 140.37, 139.21, 138.67, 138.53, 138.47, 137.51, 137.48, 136.04, 136.02, 135.91, 135.60, 135.43, 135.41, 135.29, 135.25, 134.95, 134.88, 134.82, 134.58, 134.44, 134.31, 134.22, 133.54, 133.17, 133.11, 132.51, 132.08, 132.00, 129.94, 129.59, 129.42, 129.32, 127.76, 127.67, 127.64, 126.88, 126.46, 124.03, 123.94, 116.40, 115.54, 59.09, 33.35, 32.87, 32.43, 32.11, 30.25, 29.92, 29.26, 29.04, 26.81, 23.04, 15.14, 15.06, 14.98, 14.78, 13.73; vis-NIR (CS$_2$) λ_{max} 926 nm; MALDI-TOF MS (TPB) m/z 1109 (Sc$_3$N@C$_{80}^-$).

Selective germylation of Sc$_3$N@C$_{80}$ using **7**: A mixture of I_h and D_{5h} isomers of Sc$_3$N@C$_{80}$ (2.4 mg) and **7** (65 mg) in toluene (20 mL) was irradiated as described above for 20 h. Preparative HPLC separation with a Buckyprep-M column of the reaction mixture afforded pristine Sc$_3$N@D_{5h}-C$_{80}$ (0.7 mg) and **9** (2.4 mg).

Thermal degermylation of **9**: A solution of **9** (2.4 mg) in ODCB (5 mL) was heated at 130 °C under an argon atmosphere in a Schlenk tube in the dark for 15 h. After the removal of ODCB in vacuo, Sc$_3$N@I_h-C$_{80}$ (1.1 mg) was obtained by preparative HPLC separation using a Buckyprep-M column.

X-ray crystallography of **9**: Black block crystals suitable for X-ray diffraction were obtained using the liquid–liquid bilayer diffusion method with solutions of **9** in CS$_2$ using hexane as a poor solvent at 0 °C. Single-crystal X-ray diffraction data of **9** were collected on a Saturn70 CCD diffractometer (Rigaku Corp.) equipped with a nitrogen-gas flow low-temperature apparatus providing a constant temperature at 120 K. Crystal data for Sc$_3$N@I_h-C$_{80}$(Dep$_2$Ge)$_2$CH$_2$(**9**)·1.5(CS$_2$): C$_{122.5}$H$_{54}$Ge$_2$Sc$_3$NS$_3$: M_r = 1915.90, black block, 0.25 × 0.13 × 0.07 mm, λ = 0.71069 Å, monoclinic, space group $P2_1/n$ (no. 14), a = 19.5525(17), b = 20.9254(16), c = 19.6564(16) Å, β =111.0114(5)°, T = 120 K, V = 7506(11) Å^3, Z = 4, 168,721 reflections measured, 16,520 unique (R_{int} = 0.0572), which were used for all calculations, $2\theta_{max}$ = 54.20; min/max transmission=0.782/0.941 (numerical absorption correction applied); the structure was solved using a direct method using SIR2014 [48] and was refined with SHELXL [49]. The final $wR(F_2)$ was 0.0927 (all data), conventional R_1 = 0.0424 computed for 16,316 reflections with I >2σ (I) using 1937 parameters with 876 restraints. Crystallographic computations were performed with Yadokari-XG 2009 [50].

CCDC2127212 (**9**) contains the supplementary crystallographic data for this paper, and is obtainable free of charge from the Cambridge Crystallographic Data Centre.

Computational Methods: The computations were performed with the density functional theory (DFT) approach, namely using Becke's three parameter functional [34] combined with the non-local Lee–Yang–Parr correlation functional [35] (B3LYP). The basis set applied to H, C, N, and Si atoms is the standard 6-31G* basis [36] whereas Sc and Ge atoms are treated in the SDD basis set [37] with the SDD effective core potential (the combined basis set is coded B3LYP/6-31G*~SDD). The geometry optimizations were performed with the analytically constructed energy gradients. In the optimized B3LYP/6-31G*~SDD geometries, the electronic excitation energies were evaluated with the time-dependent (TD) DFT response-theory method [40], again at the B3LYP/6-31G*~SDD level. The computations were performed using the Gaussian 09 program package [51] (See Supplementary Materials).

Transient Absorption Spectroscopy: The excitation was performed with an amplified CPA-2110 titanium:sapphire laser (1 kHz; 150 fs pulse width; 400 nJ laser energy) from Clark-MXR Inc. EOS SYSTEM (0–10 μs) from Ultrafast Systems, working with 1 kHz pump laser at 387 nm wavelength. Probing was performed with a 2 kHz continuous white light fiber laser. Data evaluation has been conducted by means of multiwavelength and global analysis using the GloTarAn package [52].

4. Conclusions

Photoreactions of $Sc_3N@I_h$-C_{80} and **1**, **4**, and **7** afforded the corresponding 1:1 adducts, whereas $Sc_3N@D_{5h}$-C_{80} was found to be inert under identical photolytic conditions. The derivatives of $Sc_3N@I_h$-C_{80} and pristine $Sc_3N@D_{5h}$-C_{80} were separated easily by HPLC without recycling processes. In addition, pristine $Sc_3N@I_h$-C_{80} was recovered by thermolytic decomposition of the corresponding photoadducts. These procedures provide a novel method for the exclusive separation of $Sc_3N@I_h$-C_{80} and $Sc_3N@D_{5h}$-C_{80}. In laser flash photolysis experiments, the decay of transient absorption for $^3Sc_3N@I_h$-C_{80}^* was accelerated in the presence of **7**. In contrast, for $Sc_3N@D_{5h}$-C_{80}, the transient absorption was too weak to offer a basis for interaction of the corresponding triplet excited states with **7**. In turn, a meaningful conclusion regarding the reactivity differences between $Sc_3N@I_h$-C_{80} and $Sc_3N@D_{5h}$-C_{80} was hampered. It is, however, expected that the electron-transfer processes between the $^3Sc_3N@D_{5h}$-C_{80}^* and **1** are much less likely to occur than those of $Sc_3N@I_h$-C_{80}, judging from the corresponding values of changes of free energies ΔG. Therefore, the photochemical inertness of $Sc_3N@D_{5h}$-C_{80} toward **1**, **4**, and **7** might be partly attributed to the lower electron-acceptor ability of $^3Sc_3N@D_{5h}$-C_{80}^*. Further investigations of the dependence of the photochemical reactivities of EMFs on their structures including the carbon cage symmetries and the encapsulated metals are in progress.

Supplementary Materials: The following supporting information can be downloaded at: https://www.mdpi.com/article/10.3390/photochem2010010/s1, Materials and General Methods and Complete list of authors for Ref 51, Figure S1: HPLC profiles of the photoreaction of $Sc_3N@D_{5h}$-C_{80} with **1**, Figure S2: HPLC profiles of the thermolysis of the mixture of **2** and **3**, Figure S3: HPLC profiles of the photoreaction of $Sc_3N@D_{5h}$-C_{80} with **4**, Figure S4: HPLC profiles of the thermolysis of the mixture of **5a**, **5b**, and **6**, Figure S5: HPLC profile of the reaction mixture of $Sc_3N@I_h$-C_{80} and **7**, Figure S6: HPLC profiles of the photolysis of $Sc_3N@D_{5h}$-C_{80} with **7**, Figure S7: HPLC profiles of the thermolysis of **9**, Figure S8: 500 MHz ^1H NMR spectrum of **9** recorded at 293 K in CS_2/$CDCl_3$ (1:3), Figure S9: 125 MHz ^{13}C NMR spectra of **9** recorded at 293 K in CS_2/$CDCl_3$ (1:3), Figure S10: 500 MHz VT ^1H NMR spectra of **9** recorded in toluene-d_8, Figure S11: Disorder of C_{80} cage and Sc_3N cluster with occupancies in the crystal of **9**, Figure S12: Raw data of all the transient absorption measurements of $Sc_3N@I_h$-C_{80}, Figure S13: Residual measurements of $Sc_3N@I_h$-C_{80} in the absence and the presence of **7**, Figure S14: Raw data of all the transient absorption measurements of $Sc_3N@D_{5h}$-C_{80}, Figure S15: Residual measurements of $Sc_3N@D_{5h}$-C_{80} in the absence and the presence of **7**, Figure S16: UV-Visible Spectra of $Sc_3N@I_h$-C_{80} and $Sc_3N@D_{5h}$-C_{80} in toluene, Figure S17: Pure toluene reference measurements, Table S1: Ten lowest excited states of $Sc_3N@I_h$-C_{80} calculated by

TD-B3LYP/6-31G*~SDD, Figure S18: Selected molecular orbitals of $Sc_3N@I_h$-C_{80}, Table S2: Ten lowest excited states of $Sc_3N@D_{5h}$-C_{80} calculated by TD-B3LYP/6-31G*~SDD, Figure S19: Selected molecular orbitals of $Sc_3N@D_{5h}$-C_{80}, Table S3: Cartesian coordinates of optimized structures.

Author Contributions: M.K. and T.A. conceived and designed the experiments; K.M., S.F. and S.K. performed the photoreactions and characterized the products; M.Y. (Masanori Yasui) and K.M. conducted the X-ray crystallography; M.Y. (Michio Yamada) and Y.M. contributed to the analysis of the products; I.P. and D.M.G. conducted the transient absorption spectroscopy; Z.S., F.U. and L.A. performed the calculations; M.K., M.F., S.N. and T.A. wrote the paper. All authors have read and agreed to the published version of the manuscript.

Institutional Review Board Statement: Not applicable.

Informed Consent Statement: Not applicable.

Data Availability Statement: Not applicable.

Conflicts of Interest: The authors declare no conflict of interest.

References and Notes

1. Akasaka, T.; Nagase, S. (Eds.) *Endofullerenes: A New Family of Carbon Clusters*; Kluwer: Dordrecht, The Netherlands, 2002.
2. Dunsch, L.; Yang, S. Metal nitride cluster fullerenes: Their current state and future prospects endohedral fullerenes. *Small* **2007**, *8*, 1298–1320. [CrossRef]
3. Chaur, M.N.; Melin, F.; Ortiz, A.L.; Echegoyen, L. Chemical, electrochemical, and structural properties of endohedral metallofullerenes. *Angew. Chem. Int. Ed.* **2009**, *48*, 7514–7538. [CrossRef]
4. Yamada, M.; Akasaka, T.; Nagase, S. Endohedral metal atoms in pristine and functionalized fullerene cages. *Acc. Chem. Res.* **2010**, *43*, 92–102. [CrossRef]
5. Akasaka, T.; Wudl, F.; Nagase, S. (Eds.) *Chemistry of Nanocarbons*; Wiley: Chichester, UK, 2010.
6. Maeda, Y.; Tsuchiya, T.; Lu, X.; Takano, Y.; Akasaka, T.; Nagase, S. Current progress on the chemical functionalization and supramolecular chemistry of M@C_{82}. *Nanoscale* **2011**, *3*, 2421–2429. [CrossRef]
7. Lu, X.; Akasaka, T.; Nagase, S. Chemistry of endohedral metallofullerenes: The role of metals. *Chem. Commun.* **2011**, *47*, 5942–5957. [CrossRef]
8. Lu, X.; Feng, L.; Akasaka, T.; Nagase, S. Current status and future developments of endohedral metallofullerenes. *Chem. Soc. Rev.* **2012**, *41*, 7723–7760. [CrossRef]
9. Zhang, J.; Stevenson, S.; Dorn, H.C. Trimetallic nitride template endohedral metallofullerenes: Discovery, structural characterization, reactivity, and applications. *Acc. Chem. Res.* **2013**, *46*, 1458–1557. [CrossRef]
10. Rivera-Nazario, D.M.; Pinzón, J.R.; Stevenson, S.; Echegoyen, L.A. Buckyball maracas: Exploring the inside and outside properties of endohedral fullerenes. *J. Phys. Org. Chem.* **2013**, *26*, 194–205. [CrossRef]
11. Yamada, M.; Akasaka, T.; Nagase, S. Carbene additions to fullerenes. *Chem. Rev.* **2013**, *113*, 7209–7264. [CrossRef]
12. Lu, X.; Akasaka, T.; Nagase, S. Carbide cluster metallofullerenes: Structure, properties, and possible origin. *Acc. Chem. Res.* **2013**, *46*, 1627–1635. [CrossRef]
13. Popov, A.A.; Yang, S.; Dunsch, L. Endohedral fullerenes. *Chem. Rev.* **2013**, *113*, 5989–6113. [CrossRef]
14. Nagase, S. Theory and calculations of molecules containing heavier main group elements and fullerenes encaging transition metals: Interplay with experiment. *Bull. Chem. Soc. Jpn.* **2014**, *87*, 167–195. [CrossRef]
15. Yamada, M.; Akasaka, T. Emergence of highly elaborated π-space and extending its functionality based on nanocarbons: New vistas in the fullerene world. *Bull. Chem. Soc. Jpn.* **2014**, *87*, 1289–1314. [CrossRef]
16. Kako, M.; Nagase, S.; Akasaka, T. Functionalization of Endohedral Metallofullerenes with Reactive Silicon and Germanium Compounds. *Molecules* **2017**, *22*, 1179. [CrossRef]
17. Yamada, M.; Liu, M.T.H.; Nagase, S.; Akasaka, T. New Horizons in Chemical Functionalization of Endohedral Metallofullerenes. *Molecules* **2020**, *25*, 3626. [CrossRef]
18. Duchamp, J.C.; Demortier, A.; Fletcher, K.R.; Dorn, D.; Iezzi, E.B.; Glass, T.; Dorn, H.C. An isomer of the endohedral metallofullerene $Sc_3N@C_{80}$ with D_{5h} symmetry. *Chem. Phys. Lett.* **2003**, *375*, 655–659. [CrossRef]
19. Krause, M.; Dunsch, L. Isolation and Characterization of Two $Sc_3N@C_{80}$ Isomers. *ChemPhysChem* **2004**, *5*, 1445–1449. [CrossRef]

20. Wang, Z.; Omachi, H.; Shinohara, H. Non-Chromatographic Purification of Endohedral Metallofullerenes. *Molecules* **2017**, *22*, 718. [CrossRef]

21. Cai, T.; Xu, L.; Anderson, M.R.; Ge, Z.; Zuo, T.; Wang, X.; Olmstead, M.M.; Balch, A.L.; Gibson, H.W.; Dorn, H.C. Structure and Enhanced Reactivity Rates of the D_{5h} Sc$_3$N@C$_{80}$ and Lu$_3$N@C$_{80}$ Metallofullerene Isomers: The Importance of the Pyracylene Motif. *J. Am. Chem. Soc.* **2006**, *128*, 8581–8589. [CrossRef]

22. Stevenson, S.; Mackey, M.A.; Coumbe, C.E.; Phillips, J.P.; Elliott, B.; Echegoyen, L. Rapid Removal of D_{5h} Isomer Using the "Stir and Filter Approach" and Isolation of Large Quantities of Isomerically Pure Sc$_3$N@C$_{80}$ Metallic Nitride Fullerenes. *J. Am. Chem. Soc.* **2007**, *129*, 6072–6073. [CrossRef]

23. Stevenson, S.; Mackey, M.A.; Pickens, J.E.; Stuart, M.A.; Confait, B.S.; Phillips, J.P. Selective Complexation and Reactivity of Metallic Nitride and Oxometallic Fullerenes with Lewis Acids and Use as an Effective Purification Method. *Inorg. Chem.* **2009**, *48*, 11685–11690. [CrossRef]

24. Cerón, M.R.; Li, F.F.; Echegoyen, L. An efficient method to separate Sc$_3$N@C$_{80}$ I_s and D_{5h} isomers and Sc$_3$N@C$_{78}$ by selective oxidation with acetylferrocenium [Fe(COCH$_3$C$_5$H$_4$)Cp]$^+$. *Chem. Eur. J.* **2013**, *19*, 7410–7415. [CrossRef]

25. Cerón, M.R.; Izquierdo, M.; Alegret, N.; Valdez, J.A.; Rodríguez-Fortea, A.; Olmstead, M.M.; Balch, A.L.; Poblet, J.M.; Echegoyen, L. Reactivity differences of Sc$_3$N@C$_{2n}$ (2n = 68 and 80). Synthesis of the first methanofullerene derivatives of Sc$_3$N@D_{5h}-C$_{80}$. *Chem. Commun.* **2016**, *52*, 64–67. [CrossRef]

26. Kako, M.; Sugiura, T.; Akasaka, T. Photochemical addition of silirane to endohedral metallofullerene: Electronic properties of carbosilylated Sc$_3$N@I_h-C$_{80}$. *Phosphorus Sulfur Silicon Relat. Elem.* **2016**, *191*, 201–206. [CrossRef]

27. Kako, M.; Sugiura, T.; Miyabe, K.; Yasui, M.; Yamada, M.; Maeda, Y.; Guo, J.-D.; Nagase, S.; Akasaka, T. Preparation, Structural Determination, and Characterization of Electronic Properties of [5,6]- and [6,6]-Carbosilylated Sc$_3$N@I_h-C$_{80}$. *Chem. Asian J.* **2017**, *12*, 1391–1399. [CrossRef]

28. Sato, K.; Kako, M.; Mizorogi, N.; Tsuchiya, T.; Akasaka, T.; Nagase, S. Bis-silylation of Lu$_3$N@I_h-C$_{80}$: Considerable variation in the electronic structures. *Org. Lett.* **2012**, *14*, 5908–5911. [CrossRef]

29. Kako, M.; Miyabe, M.; Sato, K.; Suzuki, M.; Mizorogi, N.; Wang, W.-W.; Yamada, M.; Maeda, Y.; Olmstead, M.M.; Balch, A.L.; et al. Preparation, structural determination, and characterization of electronic properties of bis-silylated and bis-germylated Lu$_3$N@I_h-C$_{80}$. *Chem. Eur. J.* **2015**, *21*, 16411–16420. [CrossRef]

30. Han, A.H.; Wakahara, T.; Maeda, Y.; Akasaka, T.; Fujitsuka, M.; Ito, O.; Yamamoto, K.; Kako, M.; Kobayashi, K.; Nagase, S. A new method for separating the D_3 and C_{2v} isomers of C$_{78}$. *New J. Chem.* **2009**, *33*, 497–500. [CrossRef]

31. Wu, B.; Hu, J.; Cui, P.; Jiang, L.; Chen, Z.; Zhang, Q.; Wang, C.; Luo, Y. Visible-Light Photoexcited Electron Dynamics of Scandium Endohedral Metallofullerenes: The Cage Symmetry and Substituent Effects. *J. Am. Chem. Soc.* **2015**, *137*, 8769–8774. [CrossRef]

32. Wakahara, T.; Iiduka, Y.; Ikenaga, O.; Nakahodo, T.; Sakuraba, A.; Tsuchiya, T.; Maeda, Y.; Kako, M.; Akasaka, T.; Yoza, K.; et al. Characterization of the bis-silylated endofullerene Sc$_3$N@C$_{80}$. *J. Am. Chem. Soc.* **2006**, *128*, 9919–9925. [CrossRef]

33. Shriver, D.F.; Atkins, P.W.; Langford, C.H. *Inorganic Chemistry*, 2nd ed.; Oxford University Press: Oxford, UK, 1994.

34. Becke, A.D. Density-functional thermochemistry. III. The role of exact exchange. *J. Chem. Phys.* **1993**, *98*, 5648–5652. [CrossRef]

35. Lee, C.; Yang, W.; Parr, R.G. Development of the Colle-Salvetti correlation-energy formula into a functional of the electron density. *Phys. Rev. B* **1988**, *37*, 785–789. [CrossRef] [PubMed]

36. Hehre, W.J.; Ditchfield, R.; Pople, J.A. Self-consistent molecular orbital methods. XII. Further extensions of Gaussian-type basis sets for use in molecular-orbital studies of organic molecules. *J. Chem. Phys.* **1972**, *56*, 2257–2261. [CrossRef]

37. Cao, X.Y.; Dolg, M. Segmented contraction scheme for small-core lanthanide pseudopotential basis sets. *J. Mol. Struct. THEOCHEM* **2002**, *581*, 139–147. [CrossRef]

38. Pinzón, J.R.; Gasca, D.C.; Sankaranarayanan, S.G.; Bottari, G.; Torres, T.; Guldi, D.M.; Echegoyen, L. Photoinduced Charge Transfer and Electrochemical Properties of Triphenylamine I_h-Sc$_3$N@C$_{80}$ Donor-Acceptor Conjugates. *J. Am. Chem. Soc.* **2009**, *131*, 7727–7734. [CrossRef]

39. Additionally reference transient absorption measurements on pure toluene were performed (λex = 387 nm, E = 400 nJ), in order to independently prove the observed features in the respective Sc3N@Ih-C80 and Sc3N@D5h-C80 measurements (Figures 8 and 10; red species). In these measurements the exact same signal with a maximum at 555 nm could be observed, due to the very high energy density of the laser excitation, thus confirming the triplet excited state signature of toluene (Figure S17).

40. Casida, M.E.; Jamorski, C.; Casida, K.C.; Salahub, D.R. Molecular excitation energies to high-lying bound states from time-dependent density-functional response theory: Characterization and correction of the time-dependent local density approximation ionization threshold. *J. Chem. Phys.* **1998**, *108*, 4439–4449. [CrossRef]

41. Kasha, M. Characterization of electronic transitions in complex molecules. *Disc. Faraday Soc.* **1950**, *9*, 14–19. [CrossRef]

42. Akasaka, T.; Maeda, Y.; Wakahara, T.; Okamura, M.; Fujitsuka, M.; Ito, O.; Kobayashi, K.; Nagase, S.; Kako, M.; Nakadaira, Y.; et al. Novel Metal-free bis-silylation: C$_{60}$-sensitized reaction of disilirane with benzonitrile. *Org. Lett.* **1999**, *1*, 1509–1512. [CrossRef]

43. The ΔG values were calculated according to the Rehm-Weller equation [44] as follows: ΔG (kcal/mol) = 23.06[E^{ox}(D/D$^+$) − E^{red}(A/A$^-$) − ΔE^* + ε], where E^{ox}(D/D$^+$), Ered(A/A$^-$), and ΔE^* respectively represent the oxidation potential of electron-donor, the reduction potential of electron-acceptor, and the energies of excited states of electron-acceptors. Coulombic interaction energy ε in toluene (0.74) was calculated according to methods described in the literatures [46,47].

44. Rehm, D.; Weller, A. Kinetics of Fluorescence Quenching by Electron and H-Atom Transfer. *Isr. J. Chem.* **1970**, *8*, 259–271. [CrossRef]

45. Nagatsuka, J.; Sugitani, S.; Kako, M.; Nakahodo, T.; Mizorogi, N.; Ishitsuka, M.O.; Maeda, Y.; Tsuchiya, T.; Akasaka, T.; Gao, X.; et al. Photochemical addition of C_{60} with siliranes: Synthesis and characterization of carbosilylated and hydrosilylated C_{60} derivatives. *J. Am. Chem. Soc.* **2010**, *132*, 12106–12120. [CrossRef]

46. Mattay, J.; Runsink, J.; Rumbach, T.; Ly, C.; Gersdorf, J. Selectivity and charge transfer in photoreactions of donor-acceptor systems. 5. Selectivity and Charge Transfer in Photoreactions of α, α, α-Trifluorotoluene with Olefins. *J. Am. Chem. Soc.* **1985**, *107*, 2557–2558. [CrossRef]

47. Mattay, J.; Runsink, J.; Gersdorf, J.; Rumbach, T.; Ly, C. Selectivity and charge transfer in photoreactions of α,α,α-trifluorotoluene with olefins. *Helv. Chem. Acta* **1986**, *69*, 442–455. [CrossRef]

48. Burla, M.C.; Caliandro, R.; Carrozzini, B.; Cascarano, G.L.; Cuocci, C.; Giacovazzo, C.; Mallamo, M.; Mazzone, A.; Polidori, G. Crystal structure determination and refinement via SIR2014. *J. Appl. Cryst.* **2015**, *48*, 306–309. [CrossRef]

49. Sheldrick, G.M. Crystal structure refinement with SHELXL. *Acta Cryst.* **2015**, *C71*, 3–8.

50. Kabuto, C.; Akine, S.; Nemoto, T.; Kwon, E. Release of Software (Yadokari-XG 2009) for Crystal Structure Analyses. *J. Cryst. Soc. Jpn.* **2009**, *51*, 218–224. [CrossRef]

51. Frisch, M.J.; Trucks, G.W.; Schlegel, H.B.; Scuseria, G.E.; Robb, M.A.; Cheeseman, J.R.; Scalmani, G.; Barone, V.; Mennucci, B.; Petersson, G.A.; et al. *Gaussian 09, Rev. C.01*; Gaussian Inc.: Wallingford, CT, USA, 2013; (See Supplementary Materials for the complete list of authors.).

52. Snellenburg, J.J.; Laptenok, S.P.; Seger, R.; Mullen, K.M.; van Stokkum, I.H.M. Glotaran: A Java-Based Graphical User Interface for the R Package TIMP. *J. Stat. Softw.* **2012**, *49*, 1–22. [CrossRef]